11th International Symposium on Turbulence and Shear Flow Phenomena (TSFP11)
Southampton, UK, July 30 to August 2, 2019

MODELLING THE EFFECT OF TEXTURED SUPERHYDROPHOBIC SURFACES ON DRAG REDUCTION

W. Xie
Department of Engineering
University of Cambridge
Trumpington Street, Cambridge CB2 1PZ
wx233@cam.ac.uk

C. T. Fairhall
Department of Engineering
University of Cambridge
Trumpington Street, Cambridge CB2 1PZ
ctf25@cam.ac.uk

R. García-Mayoral
Department of Engineering
University of Cambridge
Trumpington Street, Cambridge CB2 1PZ
r.gmayoral@eng.cam.ac.uk

ABSTRACT

We show that turbulence over textured superhydrophobic surfaces experiences the surface as a homogeneous slip-length boundary condition. This is the case even for texture sizes $L^+ \gtrsim 10$, for which it had been previously reported that the tangential velocity and shear lost correlation. However, for sufficiently large texture sizes, $L^+ \gtrsim 25$, a non-linear interaction develops between the texture-induced flow and the overlying turbulence that modifies the dynamics of the latter. This non-linear interaction increases the Reynolds stress and the drag. To model this effect in numerical simulations, without needing to fully resolve the surface texture, we propose adding a forcing term in the governing equations, in addition to the slip boundary conditions. The texture-coherent flow, which the forcing term would depend on, can be predicted from the results of laminar simulations.

INTRODUCTION

Superhydrophobic surfaces combine surface micro-roughness with chemical hydrophobicity. This combination allows pockets of gas to be entrapped between the surface roughness elements when submerged in water. These surfaces have been shown to have a potential to reduce drag under experimental conditions, in both laminar (Ou *et al.*, 2004) and turbulent flows (Daniello *et al.*, 2009), as well as in idealised numerical simulations (Min & Kim, 2004; Martell *et al.*, 2009). Drag reduction results from the entrapped gas pockets at the surface allowing the overlying flow to locally slip.

The drag-reducing performance of superhydrophobic surfaces can be characterised through the concept of slip lengths. By considering the mean velocity at the surface, a slip length is introduced through a Navier slip condition,

$$U_s = \ell_x \left| \frac{\partial U}{\partial y} \right|_w \tag{1}$$

where U_s is the slip velocity, $\left|\frac{\partial U}{\partial y}\right|_w$ is the wall-normal gradient of the mean velocity at the surface and ℓ_x is the mean slip length. The latter is a parameter that depends on the surface texture and has been analytically derived for textures consisting of streamwise- and spanwise-aligned ridges, among others, in the Stokes regime (Philip, 1972; Lauga & Stone, 2003), and can be obtained using scaling laws for textures of posts in the same regime (Ybert *et al.*, 2007). The slip lengths obtained in the viscous regime have been shown to hold in turbulent flows for small texture sizes, $L^+ \lesssim 10$ (Seo & Mani, 2016), where L^+ is the texture spacing in wall units. For larger L^+, the slip length deviates from the viscous prediction. Seo & Mani (2016) attributed this deviation to the development of boundary layers over the roughness elements. They proposed a model, for sufficiently large texture sizes, $L^+ \gtrsim 100$, where the slip length scales with the cube root of the texture size.

Streamwise slip shifts the mean velocity profile by the slip velocity, reducing the drag. Under turbulent conditions the spanwise slip length also affects the drag. Spanwise slip allows quasi-streamwise vortices, an essential part of the near-wall turbulent cycle, to move closer to the surface (Min & Kim, 2004; Luchini, 2015), increasing the drag. Fairhall & García-Mayoral (2018) showed that for surfaces modelled using slip lengths, ΔU^+ is given by

$$\Delta U^+ \approx \ell_x^+ - \ell_T^+ \tag{2}$$

where ℓ_T^+ is the virtual origin perceived by the turbulent flow (Gómez-de-Segura *et al.*, 2018; García-Mayoral *et al.*, 2018). For surfaces where homogeneous slip lengths are applied, Fairhall & García-Mayoral (2018) proposed

$$\ell_T^+ \approx \frac{\ell_z^+}{1 + \ell_z^+/4} \tag{3}$$

from an emperical fit of the results of Busse & Sandham (2012). The drag-reducing mechanism of (Eq. 2) is the same proposed by (Luchini *et al.*, 1991; Luchini, 1996) for

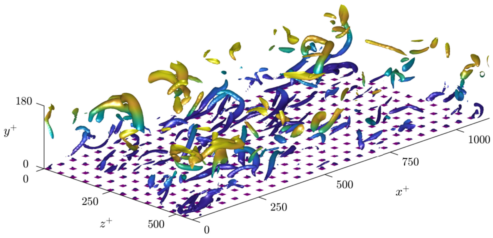

Figure 1. Instantaneous realisation of vortical structures, represented using the Q-criterion, showing the surface texture for the case $L^+ = 47$.

riblets, where ΔU^+ was shown to be proportional to the difference between streamwise and spanwise slip lengths.

NUMERICAL METHOD

We conduct direct numerical simulations (DNSs) of channels with textured superhydrophobic surfaces on both channel walls. No-slip is applied over the roughness crests, with the gas pockets modelled by a free-slip condition and considered rigid, resulting in an impermeability condition at the surface. The surface texture consists of a regular array of square posts in a collocated arrangement, shown in figure 1, with a solid fraction, the ratio between the area of the texture posts and total surface area, of $\phi_s = 1/9$. This is the same texture pattern as in Seo & Mani (2016). We study three texture sizes, $L^+ = 12-47$.

The flow within the channel is governed by the three-dimensional incompressible Navier-Stokes equations,

$$\nabla \cdot \boldsymbol{u} = 0, \tag{4}$$

$$\frac{\partial \boldsymbol{u}}{\partial t} + \boldsymbol{u} \cdot \nabla \boldsymbol{u} = -\nabla p + \frac{1}{\mathrm{Re}} \nabla^2 \boldsymbol{u}, \tag{5}$$

where $\boldsymbol{u}$ is the velocity vector with components u, v, w in the streamwise, x, wall-normal, y, and spanwise, z, directions respectively, p is the kinematic pressure, and Re is the bulk Reynolds number.

The channel is periodic in the streamwise and spanwise directions, with these directions discretised spectrally. The wall-normal direction is discretised using second-order finite differences on a staggered grid. A fractional step method (Kim & Moin, 1985), combined with a three-step Runge-Kutta scheme, is used to advance in time with a semi-implicit scheme used for the viscous terms and an explicit scheme for the advective terms. All simulations were run at a friction Reynolds number $\mathrm{Re}_\tau \approx 180$, with a few verification simulations at $\mathrm{Re}_\tau \approx 405$, by applying a constant mean pressure gradient. The channel is of size $2\pi\delta \times \pi\delta \times 2\delta$ in the streamwise, spanwise and wall-normal directions respectively, where δ is the channel half-height. Statistics were obtained by averaging over a period of approximately 10 eddy-turnovers after statistical convergence had been reached. Further details of the numerical method can be found in Fairhall & García-Mayoral (2018). The simulation parameters are given in the Table 1.

Slip-Length Simulations vs. Textured Simulations

Seo & Mani (2016) investigated the limits of slip-length models, and showed that for texture sizes $L^+ \gtrsim 10$, the instantaneous correlation between velocity and shear, implicit in the Robin boundary condition of equation 1, was lost. This would appear to set the upper limit for the applicability of a slip-length model. They also observed that for sufficiently large texture size, ΔU^+ obtained from texture-resolved simulations is smaller than that predicted from slip-length models. Fairhall & García-Mayoral (2018) later investigated slip-length correlation using a spectral approach to discriminate between the slip length experienced by different lengthscales in the overlying flow. The slip length in a spectral framework is characterised by both a magnitude and a phase, with the phase having streamwise and spanwise components. The phase of the slip length, φ, represents the phase lag between the velocity and shear at the surface. For a given wavelength, λ, the phase is $\varphi = 2\pi\Delta/\lambda$, where Δ is the spatial offset between the velocity and shear. For a homogeneous slip-length model to be valid, the measured slip length should have a magnitude that is constant in time and across wavelengths, with the velocity and shear in phase. In the following discussion, two slip lengths will be referred to, the mean slip length and the dynamic slip length. The mean slip length, $\overline{\ell}_x^+$, is the time-average of the slip length experienced by the streamwise zero mode, i.e. it is the slip length experienced by the mean velocity profile. The dynamic slip length, $\hat{\ell}^+$, is the time-average slip length experienced by the velocity fluctuations (Seo & Mani, 2016). The dynamic slip length is obtained from a linear regression of the instantaneous velocity and shear fluctuations. Fairhall & García-Mayoral (2018) showed that even scales much larger than the texture size displayed an apparent loss of correlation, not just scales of the order of the texture size. This is demonstrated in figure 2 (a-d), which shows the slip lengths obtained for surface with a texture size $L^+ \approx 47$. Fairhall & García-Mayoral (2018) proposed that this observed loss of correlation of the slip length was due to the texture-induced flow becoming of the same order as the overlying turbulent flow. The texture-induced flow is modulated in intensity by the overlying flow, which scatters the texture-induced signal across the full range of lengthscales. Therefore, to better assess the slip length perceived by the overlying turbulence, the texture-induced flow needs to be filtered from the velocity fields.

Table 1. Simulation parameters for texture-resolving simulations, cases $T12$, $T24$ and $T47$, and homogeneous-slip simulations, cases $S12$, $S24$ and $S47$. L^+ is the texture size, ℓ_x^+ and ℓ_z^+ are the streamwise and spanwise slip lengths, and ΔU^+ is the resulting shift of the logarithmic region of the mean velocity profile.

Case	L^+	ℓ_x^+	ℓ_z^+	ΔU^+
$T12$	12	3.8	2.9	2.1
$T24$	24	6.9	4.4	4.0
$T47$	47	10.0	6.4	5.4
$S12$	–	3.8	2.9	2.2
$S24$	–	6.9	4.3	5.0
$S47$	–	10.0	6.3	7.7

Amplitude-Modified Triple Decomposition

Triple decomposition (Reynolds & Hussain, 1972) is commonly used to separate a 'texture-coherent' contri-

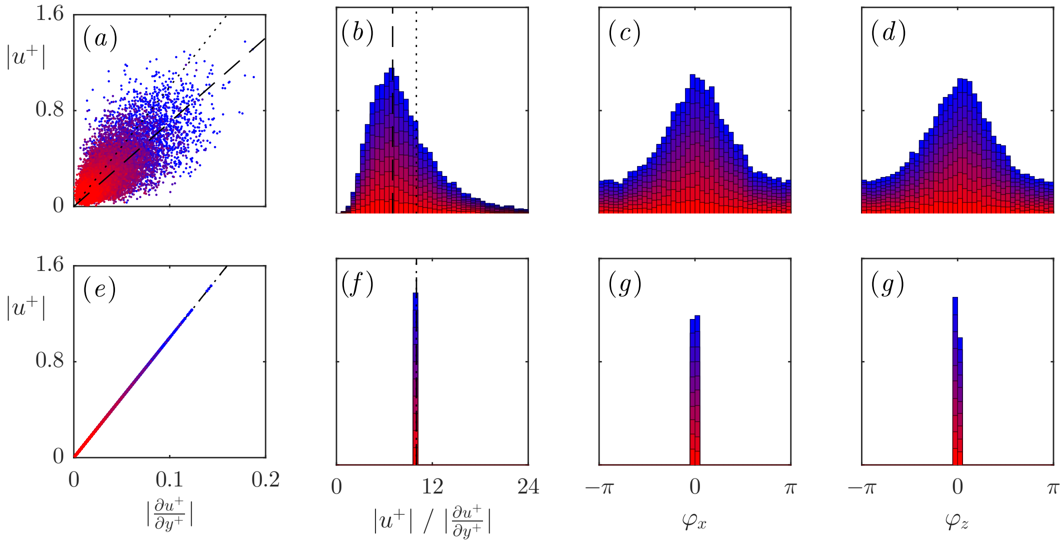

Figure 2. Instantaneous streamwise slip lengths obtained from the full velocity fields (top) and the turbulent component isolated from the flow-fields (bottom) for wavelengths $\lambda_x^+ \approx 113 - 1131$ and $\lambda_z^+ \approx 113 - 565$ (coloured from red to blue for increasing streamwise wavelength) for a texture size $L^+ \approx 47$. (*a*,*e*) instantaneous correlation of velocity and shear magnitudes; (*b*,*f*) probability density histogram of the slip length; (*c*,*g*) streamwise and (*d*,*h*) spanwise phase difference between velocity and shear. In (*a*,*b*,*e*,*f*) the dashed line indicates the fitted dynamic slip length, obtained from a linear regression of the data points, and the dotted line indicates the mean slip length.

bution from the texture-incoherent, overlying turbulence. This decomposition splits the flow field into a space-time-averaged mean flow, a time-averaged component which is phase-locked to the texture, and the remaining time-space fluctuations,

$$\begin{aligned} u(x,y,z,t) &= U(y) + u'(x,y,z,t) \\ &= U(y) + \widetilde{u}_u(\widetilde{x},y,\widetilde{z}) + u_T(x,y,z,t). \end{aligned} \tag{6}$$

Here, $U(y)$ is the mean velocity at a given height and $u'(x,y,z,t)$ is the total fluctuation. The latter is further decomposed into the texture-coherent fluctuation $\widetilde{u}_u(\widetilde{x},y,\widetilde{z})$, where $\widetilde{x}$ and $\widetilde{z}$ refer to the local coordinates within the texture period, and the remaining fluctuation $u_T(x,y,z,t)$. However, it was shown by Abderrahaman-Elena & García-Mayoral (2016) that this decomposition is not completely effective at filtering out the texture-induced flow from u_T for textured surfaces. They showed that the texture-coherent flow was modulated in intensity by the overlying turbulent flow, and proposed a modification to the triple decomposition to account for this modulation,

$$\begin{aligned} u(x,y,z,t) \approx &U(y) + \widetilde{u}_u(\widetilde{x},y,\widetilde{z}) \left(\frac{U(y) + u_T(x,y,z,t)}{U(y)} \right) \\ &+ u_T(x,y,z,t). \end{aligned} \tag{7}$$

Abderrahaman-Elena & García-Mayoral (2016) showed that this modified form of the triple decomposition was more effective at removing the footprint of the texture from u_T.

The same principle of modulation of the texture-coherent flow by the overlying turbulence can be applied to the spanwise velocity. Further details of this decomposition can be found in Abderrahaman-Elena *et al.* (2019).

The result of the above decomposition minimises the signature of the texture in u_T and w_T. These will be referred to as the 'turbulent' components in the following discussions. Instantaneous flow fields for the full streamwise and spanwise velocities at the surface for the case with $L^+ \approx 12$ are shown in figure 3, together with the turbulent velocity fields obtained from both the conventional triple decomposition and the modified decomposition of equation (7).

Slip length perceived by the background turbulence

After isolating the background turbulent component of the flow using the decomposition of equation (7), Fairhall *et al.* (2019) reassessed the apparent slip length experienced by the turbulent lengthscales in the overlying flow. The velocity-shear correlations of the background turbulent components, u_T and w_T are shown in figure 2 (e-g). These figures show an essentially linear correlation between velocity and shear, with little scatter, so that a slip-length can meaningfully be defined. It should be noted that the use of the conventional triple decomposition to filter the flow fields would yield the same correlations of figure 2(a-d). This is because the wavelengths portrayed, λ_x^+, $\lambda_z^+ > 100$ are larger than the texture wavelength, and would therefore be unmodified by the decomposition. The recovery of the slip length correlation for u_T and w_T can be interpreted as the overlying, background turbulence being subject to a homogeneous slip boundary condition. The loss of correlation previously observed would be the result of contamination by the texture-induced flow. Further to this, the streamwise dynamic slip length, i.e. the slip length experienced by the velocity fluctuations, recovers the value of the mean slip length, in contrast with the smaller value obtained from the full velocity signal. The previously observed reduction in value, therefore, also appears to be a result of contamination by the texture-induced flow. The spanwise fluctuations, however, still appear to experience a slip length smaller than the mean streamwise one, despite the isotropy of the texture, even if the spanwise velocity and shear are also well correlated.

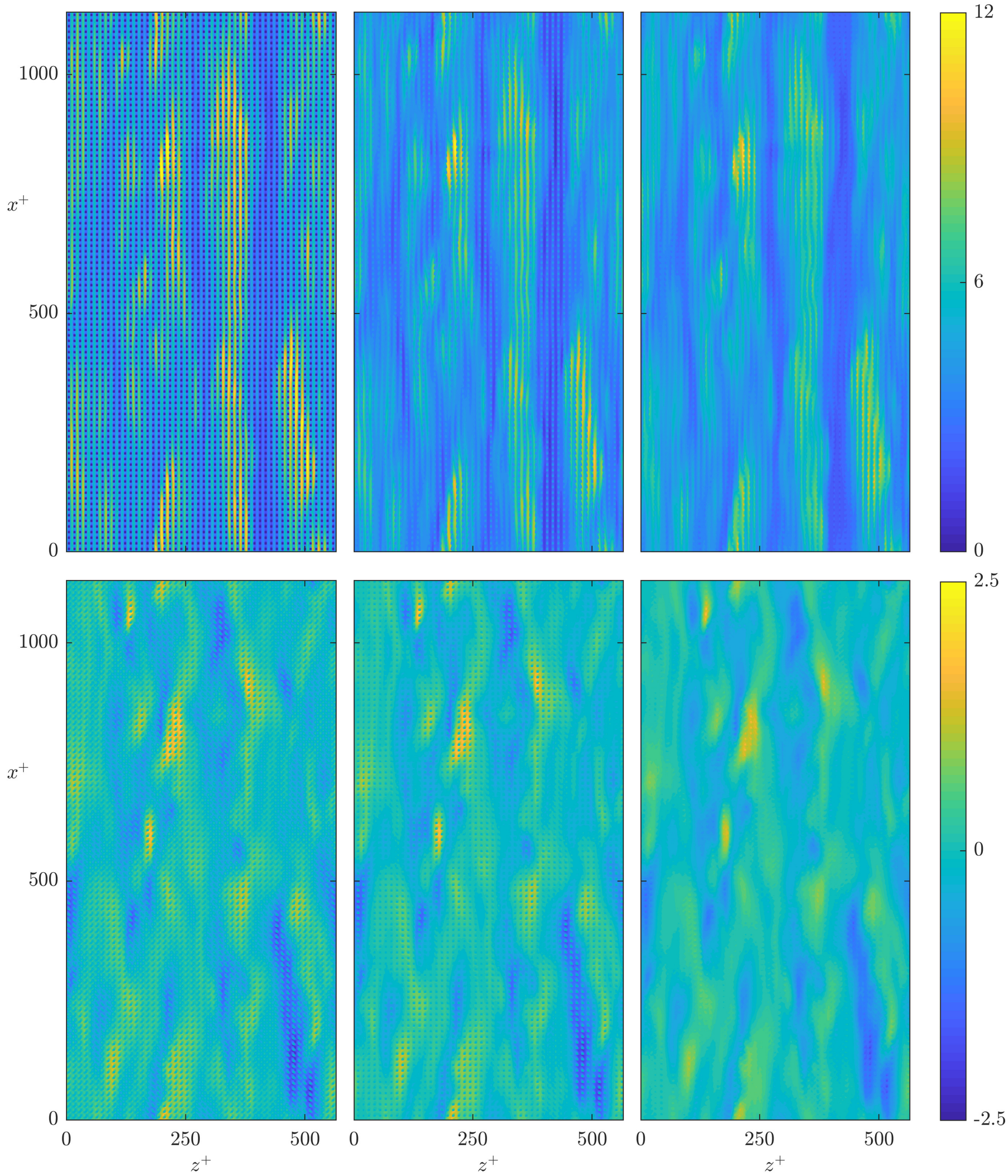

Figure 3. Streamwise (top) and spanwise (bottom) instantaneous velocity snapshots for the full velocity field (left), the turbulent component obtained from the conventional triple decomposition (middle) and the turbulent component obtained from the modified triple decomposition (right) for the case with $L^+ \approx 12$.

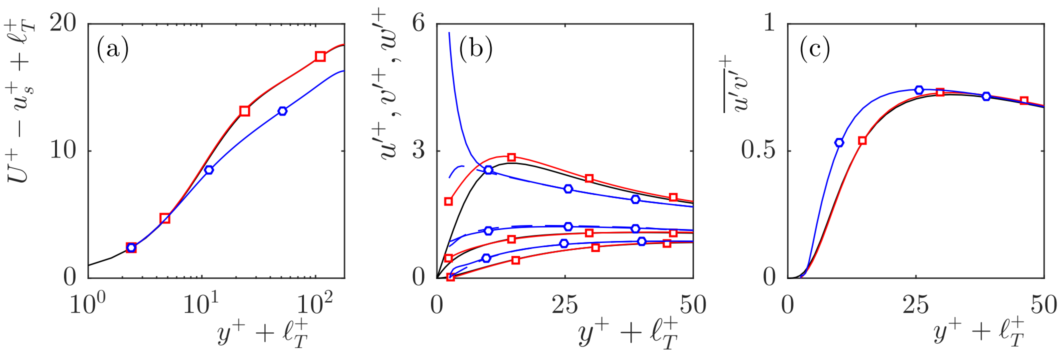

Figure 4. Comparison of textured and homogenous fluctuations with smooth channel data for the cases with $L^+ \approx 47$. (*a*) mean velocity profile; (*b*) rms velocity fluctuations (*c*) Reynolds stress fluctuations. —, smooth channel; —□—, homogeneous slip-length simulations; —○—, full velocity of textured simulations; – –, turbulent component of textured simulations.

Additional Drag Resulting from the Granularity of the Surface Texture

To investigate the discrepancy in ΔU^+ for larger texture sizes, the results of texture-resolving simulations are compared to simulations with homogeneous slip-lengths. We assume that the effect of the surface on the overlying flow is effectively imposing slip boundary conditions, $u_s = \ell_x \left|\partial u/\partial y\right|_w$ and $w_s = \ell_z \left|\partial w/\partial y\right|_w$.

Consequently, we assume that the virtual origins of the mean flow, ℓ_x^+, and the turbulent flow, ℓ_T^+, in textured simulations are the same as those in the corresponding homogeneous simulation. Any further changes to the flow, compared to the homogeneous cases, would then be a consequence of the granularity of textured surfaces.

The mean velocity profile, rms velocity fluctuations and Reynolds stress for a texture size $L^+ \approx 47$, and a simulation using the observed slip lengths as homogeneous boundary conditions are shown in figure 4. Note that these results have been shifted in y^+ by ℓ_T^+ and scaled by the friction velocity at $y^+ = -\ell_T^+$, the region perceived by the overlying turbulence (Fairhall *et al.*, 2019). The homogeneous slip-length simulations collapse to the smooth channel data, indicating essentially no change in the turbulent dynamics beyond the change of perceived origin. However, the texture-resolved simulations show significantly modified profiles.

The cause of the discrepancy in ΔU^+ between the two simulations can be investigated by integrating the streamwise momentum equation (García-Mayoral & Jiménez, 2011). Fairhall (2019) showed that for a textured superhydrophobic surface this gives

$$\Delta U^+ \approx \ell_x^+ - \ell_T^+ - \int_{\ell_T^+}^{H^+} (\tau^+_{uv,\mathrm{SHS}} - \tau^+_{uv,\mathrm{SC}})dy^+ \tag{8}$$

where τ_{uv} is the Reynolds stress for a superhydrophobic surface, subscript SHS, and smooth channel, subscript SC, respectively, and H^+ is a height sufficiently far above the surface. For simulations where slip lengths are applied, the final term in equation (8), the additional Reynolds stress integral, is zero (Fairhall *et al.*, 2019), recovering equation (2). The discrepancy between ΔU^+ between the two simulations must, therefore, arise due to modifications to the Reynolds stress profile resulting from the granularity of the surface. This is shown in figure 4(c) where the Reynolds stress profile displays an increase in Reynolds stress in the region $5 \lesssim y^+ \lesssim 25$ compared to the homogeneous slip-length simulations. The contribution of the texture-coherent component to the Reynolds stress is negligible, so the observed difference is essentially caused by modifications in the background turbulence. This difference can only be caused by the non-linear interaction of the texture-induced flow with the overlying turbulence, which modifies its dynamics and is detrimental to the drag. Homogeneous slip-length models are only able to capture the change in virtual origins of the flow, and not this non-linear interaction.

Modelling Granularity Effects in Simulations with Homogeneous Slip

The triple decomposition gives insights to model the non-linear interaction of the texture-induced flow with the overlying turbulence in texture-resolving simulations, and represent its effect in the simulations with homogeneous slip. We substitute the triple-decomposed velocity, $\boldsymbol{u} = \boldsymbol{U} + \tilde{\boldsymbol{u}} + \boldsymbol{u}_T$, and pressure, $p = P + \tilde{p} + p_T$, into the Navier-Stokes equations (5). According to Fairhall *et al.* (2019), the coherent flow of $\boldsymbol{U} + \tilde{\boldsymbol{u}}$ and $P + \tilde{p}$ satisfies Navier-Stokes equations. Hence, a momentum equation for the background turbulent fluctuations can be obtained, of the form

$$\frac{\partial \boldsymbol{u}_T}{\partial t} + \boldsymbol{u}_T \cdot \nabla \boldsymbol{u}_T + N_T = -\nabla p_T + \frac{1}{Re}\nabla^2 \boldsymbol{u}_T, \tag{9a}$$

where $N_T = (\boldsymbol{U} + \tilde{\boldsymbol{u}}) \cdot \nabla \boldsymbol{u}_T + \boldsymbol{u}_T \cdot \nabla(\boldsymbol{U} + \tilde{\boldsymbol{u}})$. For the mean flow, we obtain

$$\frac{\partial \boldsymbol{U}}{\partial t} + N_U = -\nabla P + \frac{1}{\mathrm{Re}}\nabla^2 \boldsymbol{U}, \tag{9b}$$

where $N_U = \langle(\tilde{\boldsymbol{u}} + \boldsymbol{u}_T) \cdot \nabla(\tilde{\boldsymbol{u}} + \boldsymbol{u}_T)\rangle$. N_T and N_U can be interpreted as forcing terms on Navier-Stokes equations, which represent the non-linear interaction of the texture-coherent flow with the background turbulence. Therefore, we can model the effects of granularity on the background turbulence in simulations with homogeneous slip by adding these forcing terms. We illustrate this concept with a simple example, two-dimensional laminar channel flow. In this case, $\boldsymbol{u}_T = 0$ and $p_T = 0$, and therefore $\boldsymbol{u} = \boldsymbol{U} + \tilde{\boldsymbol{u}}$ and $p = P + \tilde{p}$.

We conduct two simulations at $Re = 1000$. The first one is the fully-resolved simulation with textured surfaces, and the second one is the simulation with homogeneous-slip plus forcing terms. Both the slip length and the forcing terms in the latter are obtained from the former. In the simulation with homogeneous-slip, $\tilde{\boldsymbol{u}}$ and $\tilde{p}$ are 0, and the only component left to be solved is the mean component. In Equation (9b), the forcing term reduces in the laminar case to $N_U = \langle \tilde{\boldsymbol{u}} \cdot \nabla \tilde{\boldsymbol{u}} \rangle$.

When only homogeneous slip is imposed, the velocity profile is parabolic, Poisseuille-like. Figure (5) compares the deviations from that profile of the texture-resolving simulation and the simulation with homogeneous-slip plus the forcing term N_U. The results show that the latter can capture the effect of granularity on the background flow.

CONCLUSIONS

We have investigated the effects of granularity of a superhydrophobic surface over a range of texture sizes by conducting a series of DNSs comparing texture-resolving and homogeneous-slip layouts. We decompose the flow into background-turbulence and texture-coherent components, and show that the background-turbulence experiences the surface as homogeneous slip lengths. The validity of the slip-length model can then be extended to $L^+ \lesssim 20$, which is larger than thought previously.

For $L^+ \gtrsim 25$, however, we observe that a non-linear interaction with the texture-coherent flow develops, altering the dynamics of the background turbulence. This has the effect of reducing ΔU^+ compared to that predicted using a homogeneous slip model, and sets the upper limit of applicability of such models. To model this non-linear interaction, we add a forcing term to the momentum equation of the homogeneous-slip case, which accounts for the non-linear interaction of the texture-coherent flow and the background flow. We demonstrate the model by applying it to a laminar flow, with good results.

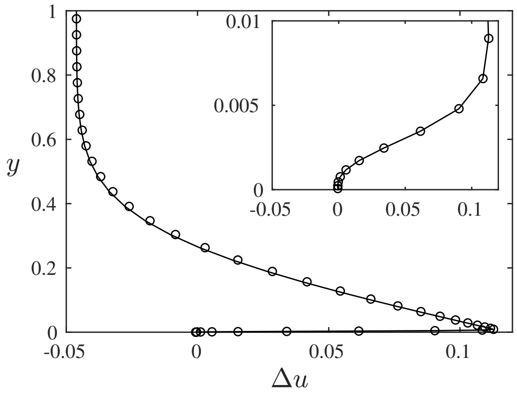

Figure 5. The comparison of the deviations from the parabolic profile of the texture-resolving simulation and the simulation with homogeneous-slip plus forcing terms. The solid curve is the difference between the mean velocity profile from the texture-resolving simulation and the parabolic velocity profile. The circles are the difference between the velocity profile from the simulation with homogeneous-slip plus forcing terms and the parabolic velocity profile.

REFERENCES

Abderrahaman-Elena, N., Fairhall, C. T. & García-Mayoral, R. 2019 Modulation of near-wall turbulence in the transitionally rough regime. *J. Fluid. Mech.* **865**, 1042–1071.

Abderrahaman-Elena, N. & García-Mayoral, R. 2016 Geometry-induced fluctuations in the transitionally rough regime. *J. Phys. Conf. Ser.* **708**, 012009.

Busse, A. & Sandham, N. D. 2012 Influence of an anisotropic slip-length boundary condition on turbulent channel flow. *Phys. Fluids* **24**, 055111.

Daniello, R. J., Waterhouse, N. E. & Rothstein, J. P. 2009 Drag reduction in turbulent flows over superhydrophobic surfaces. *Phys. Fluids* **21**, 085103.

Fairhall, C. T. 2019 The influence of superhydrophobic surfaces on near-wall turbulence. PhD thesis, University of Cambridge.

Fairhall, C. T., Abderrahaman-Elena, N. & García-Mayoral, R. 2019 The effect of slip and surface texture on turbulence over superhydrophobic surfaces. *J. Fluid. Mech.* **861**, 88–118.

Fairhall, C. T. & García-Mayoral, R. 2018 Spectral Analysis of the Slip-Length Model for Turbulence over Textured Superhydrophobic Surfaces. *Flow Turbul. Combust.* **100**, 961–978.

García-Mayoral, R., Gómez-de-Segura, G. & Fairhall, C. T. 2018 The control of near-wall turbulence through surface texturing. *Fluid Dyn. Res.* **51**, 011410.

García-Mayoral, R. & Jiménez, J. 2011 Hydrodynamic stability and breakdown of the viscous regime over riblets. *J. Fluid Mech.* **678**, 317–347.

Gómez-de-Segura, G., Fairhall, C. T., MacDonald, M., Chung, D. & García-Mayoral, R. 2018 Manipulation of near-wall turbulence by surface slip and permeability. *J. Phys. Conf. Ser.* **1001**, 012011.

Kim, J. & Moin, P. 1985 Application of a Fractional-Step Method to Incompressible Navier-Stokes Equations. *J. Comp. Phys.* **59**, 308–323.

Lauga, E. & Stone, H. A. 2003 Effective slip in pressure-driven Stokes flow. *J. Fluid Mech.* **489**, 55–77.

Luchini, P. 1996 Reducing the turbulent skin friction. In *Computational Methods in Applied Sciences – Proc. 3rd ECCOMAS CFD Conference*, pp. 466–470.

Luchini, P. 2015 The relevance of longitudinal and transverse protrusion heights for drag reduction by a superhydrophobic surface. In *European Drag Reduction and Flow Control Meeting 2015*, pp. 81–82.

Luchini, P., Manzo, F. & Pozzi, A. 1991 Resistance of a grooved surface to parallel flow and cross-flow. *J. Fluid Mech.* **228**, 87–109.

Martell, M. B., Perot, J. B. & Rothstein, J. P. 2009 Direct numerical simulations of turbulent flows over superhydrophobic surfaces. *J. Fluid Mech.* **620**, 31–41.

Min, T. & Kim, J. 2004 Effects of hydrophobic surface on skin-friction drag. *Phys. Fluids* **16**, L55–L58.

Ou, J., Perot, B. & Rothstein, J. P. 2004 Laminar drag reduction in microchannels using ultrahydrophobic surfaces. *Phys. Fluids* **16**, 4635–4643.

Philip, J. R. 1972 Flows Satisfying Mixed No-Slip and No-Shear Conditions. *Z. Angew. Math. Phys.* **23**, 353–372.

Reynolds, W. C. & Hussain, A. K. M. F. 1972 The mechanics of an organized wave in turbulent shear flow. Part 3. Theoretical models and comparisons with experiments. *J. Fluid Mech.* **54**, 263–288.

Seo, J. & Mani, A. 2016 On the scaling of the slip velocity in turbulent flows over superhydrophobic surfaces. *Phys. Fluids* **28**, 025110.

Ybert, C., Barentin, C. & Cottin-Bizonne, C. 2007 Achieving large slip with superhydrophobic surfaces: Scaling laws for generic geometries. *Phys. Fluids* **19**, 123601.